Journal Name

RSCPublishing

COMMUNICATION

High-performance symmetric sodium-ion batteries using a new bipolar material O3-type $Na_{0.8}Ni_{0.4}Ti_{0.6}O_2$

Cite this: DOI: 10.1039/xoxx00000x

Shaohua Guo,[a, b] Haijun Yu, * [a] Pan Liu,[c] Yang Ren,[d] Tao Zhang,[a] Mingwei Chen,[c] Masayoshi Ishida,[b] Haoshen Zhou *[a, b, e]

Received ooth January 2014,
Accepted ooth January 2014

DOI: 10.1039/xoxx00000x

www.rsc.org/

Based on low cost and rich resources, sodium-ion batteries have been regarded as a promising candidate for the next generation energy storage batteries in large-scale energy application for renewable energy and smart grid. However, there are some critical drawbacks limiting its application, such as safety and stability problems. In this work, a stable symmetric sodium-ion battery based on bipolar active material O3-type $Na_{0.8}Ni_{0.4}Ti_{0.6}O_2$ is developed. This bipolar material shows a typical O3-type layered structure, containing two electrochemically active transition metals with redox couples of Ni^{4+}/Ni^{2+} and Ti^{4+}/Ti^{3+}, respectively. This $Na_{0.8}Ni_{0.4}Ti_{0.6}O_2$-based symmetric cell exhibits a high voltage of 2.8 V, a reversible discharge capacity of 85 mAh g^{-1}, 75% capacity retention after 150 cycles and good rate capability. This full symmetric cell will greatly contribute to the development of room-temperature sodium-ion batteries towards safety, low cost, long life, and will stimulate further research on symmetric cells using the same active materials as both cathode and anode.

Introduction

Due to the increasing concerns about fossil fuels depletion, renewable energy such as wind and solar power has been widely developed in the modern electrical grid.[1, 2] However, renewable energy is intermittent, and it needs to be balanced and integrated into the grid smoothly and safely. To smooth out its variation over time, low-cost electrical energy storage (EES) becomes extremely necessary. Electrochemical batteries can efficiently store and release electricity in chemicals, showing the most promising in stationary applications for EES.[3] Although lithium ion batteries (LIBs) have been considered for electrical grid storage,[4-9] their limited availability and increasing cost with worldwide commercialization cannot satisfy the substantial demand. Nevertheless, sodium possessing the similar physical and chemical properties with lithium has almost infinite supply, and has attracted great attentions to develop room-temperature sodium-ion batteries (SIBs).[10-19]

Great efforts have been made in the design of SIBs with high efficiency. Layered oxide compounds ($Na_{2/3}Ni_{1/3}Ti_{2/3}O_2$, $Na_{2/3}Fe_{1/2}Mn_{1/2}O_2$, $Na_{0.85}Li_{0.17}Ni_{0.21}Mn_{0.64}O_2$)[12, 20, 21] polyanion compounds ($Na_3V_2(PO4)_3$, $Na_{1.5}VPO_{4.8}F_{0.7}$, $Na_7V_4(P_2O_7)_4PO_4$),[22-25] Prussian blue[18, 26, 27] and carbon compounds (graphite, hard carbon)[28, 29] have been extensively investigated, and computational techniques have also been applied recently to a variety of sodium-based compounds.[30-32] Most of the full sodium cells are non-symmetric, consisting of layered $NaTMO_2$ (where the transition metal (TM) is the element of V, Cr, Mn, Fe, Co and Ni) cathode[33-40] and carbon/sodium metal anode[29, 41, 42] as sodium ions "stocking chair" reaction components[43]. However, potential safety concerns on carbon materials (especially hard carbon) with possible thermal runaway are noticed because their voltage plateau related with most capacity is too close to the sodium plating voltage. This kind of SIBs system cannot support the requirement of long life and safety of large-scale energy storage devices, therefore development of new sodium storage system is necessary. [44, 45]

Recently, the full symmetric vanadium or titanium-based SIBs in terms of two TM^{4+}/TM^{3+} and TM^{3+}/TM^{2+} redox couples in $Na_3TM_2(PO_4)_3$ (TM = Ti or V) with NASICON structure have been proposed.[46-48] These symmetric SIBs are very attractive and promising from a commercial standpoint, cathode and anode with the same active materials can enable cells overcharging to some extent, buffer the large volume expansion (cathode expanding accompanied by anode shrinking, and vice versa), greatly reduce the manufacturing costs and simplify the fabrication process.[49, 50] Although, their cycle instability (only few cycles can be conducted) and low energy density (low average potential of 1.7 V) of current developed symmetric SIBs are insufficient for long-term operation in EES, preventing the further application of symmetric cells. Hence, developing bipolar materials with good cycle performance to build safe, inexpensive and long-life full symmetric SIBs is a great challenge.

In the past studies, $NaNiO_2$ and $NaTiO_2$ layered oxide can serve as cathode and anode materials of SIBs through the redox of nickel and titanium, respectively. However, complex phase transformation

COMMUNICATION

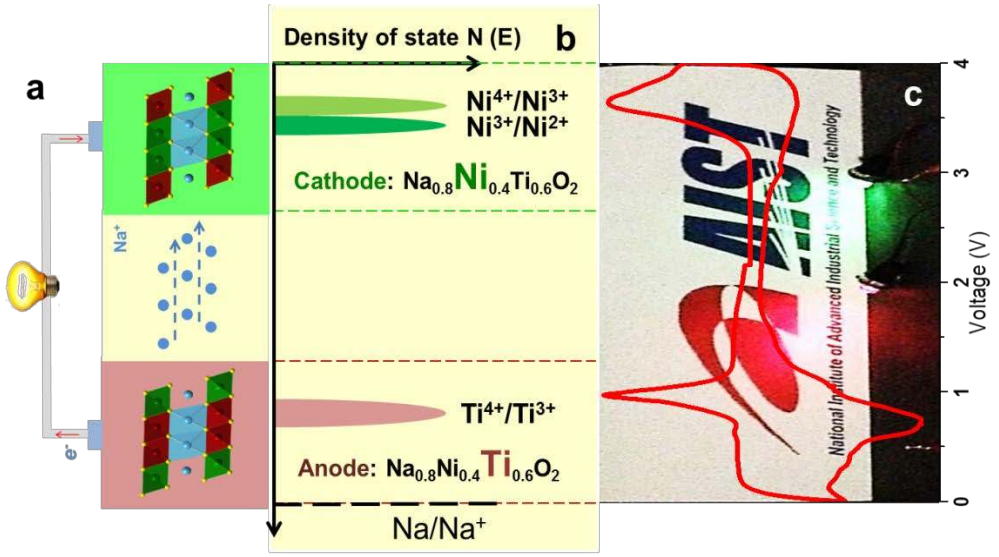

Figure 1. Schematic illustration of designing the symmetric SIBs via the two redox couples of nickel and titanium in the layered materials $Na_{0.8}Ni_{0.4}Ti_{0.6}O_2$. **(a)** A diagram of the proposed symmetric cell based on O3-type $Na_{0.8}Ni_{0.4}Ti_{0.6}O_2$. **(b)** schematic of energy *vs.* density of states plot, showing the relative positions of the Fermi energy level of Ni^{4+}/Ni^{2+} (Ni^{4+}/Ni^{3+} and Ni^{3+}/Ni^{2+}) and Ti^{4+}/Ti^{3+} redox couples for O3-type $Na_{0.8}Ni_{0.4}Ti_{0.6}O_2$. **(c)** The CV curve of $Na_{0.8}Ni_{0.4}Ti_{0.6}O_2$/Na half cell in the whole voltage range of 0-4 V *vs.* Na^+/Na, and the background shows the lighted LED bulbs driven up by the designed bipolar $Na_{0.8}Ni_{0.4}Ti_{0.6}O_2$-based symmetric cells.

with evident step-like character[38, 51] in $NaNiO_2$ material exists during their desodiation and sodiation,[52] and also the layered O3-type Na_xTiO_2 is not stable for the Ti^{3+} chemical environment.[39, 44] Our recent studies have clearly confirmed that solid-solution of $NaTMO_2$ and $NaTiO_2$ layered oxides can well improve the comprehensive electrochemical performance, especially on the cycle capability.[53, 54] Considering the similar ionic radius of nickel and titanium, we designed and synthesized the solid-solution material of O3-type $Na_{0.8}Ni_{0.4}Ti_{0.6}O_2$ without impurities, and the 'golden pair' of nickel and titanium not only greatly stabilize each other in the sodium electrochemical processes, but also exhibit the unique double redox couples of Ni^{4+}/Ni^{2+} (3.5 V) and Ti^{4+}/Ti^{3+} (0.7 V). These advantages of this bipolar material are used to implement a novel symmetric SIB. This cell exhibits a reversible discharge capacity of 85 mAh g^{-1} with the average voltage of 2.8 V. It also presents a superior long life exceeding 150 cycles with capacity retention of 75%.

Results and discussion

Figure 1a shows the schematic of proposed sodium-ion batteries, and the brown, yellow and green parts represent anode, electrolyte and cathode, respectively. In the traditional SIBs, the cathode is different from the anode to generate a certain voltage gap and supply an applicable energy density. Herein, we use the "unique" electrode of O3-type $Na_{0.8}Ni_{0.4}Ti_{0.6}O_2$ simultaneously as cathode and anode. This novel design ensures the safety, is more tolerant of overcharge, reduces the comprehensive cost and makes cell recycling more convenient.[49, 50] Figure 1b is a schematic of energy vs. density of states plot, showing the relative position of the Fermi energy level of Ni^{4+}/Ni^{2+} (Ni^{4+}/Ni^{3+} and Ni^{3+}/Ni^{2+}) and Ti^{4+}/Ti^{3+} redox couples for O3-type $Na_{0.8}Ni_{0.4}Ti_{0.6}O_2$.[5] To illustrate these redox couple, the CV curve with a wide voltage range of 0-4 V in the half cell of $Na_{0.8}Ni_{0.4}Ti_{0.6}O_2$/Na is carried out in the right of Figure 1c. It is clear that two distinct redox peaks of around 3.6/3.5 V and 0.95/0.7 V are observed, surprisingly there is a large potential difference between the two redox couples. Bivalence of nickel and tetravalence of titanium are further validated from their potentials vs. Na,[5, 44] which is also used to fabricate series of materials with different compositions.[55, 56] The results indicate that two elements (Ni and Ti) of the same materials can be simultaneously oxidized and reduced in an electrochemical process, and simulate us to develop a novel symmetric SIB. The background of Figure 1c depicts that our novel symmetric cells after charge to 3.8 V vs. Na^+/Na successfully light 2 LED lamps.

The crystal structures of the bipolar material were characterized by high-resolution synchrotron X-ray diffraction (HR-SXRD), displaying O3-type structure with high crystalline. The composition of $Na_{0.83}Ni_{0.40}Ti_{0.60}O_2$ is confirmed by Inductively Coupled Plasma Mass Sepectrometry (ICP-MS), which is closely matching the designed product. All the diffraction peaks of the bipolar material can be well indexed to rhombohedral symmetry structure with $R\bar{3}m$ space group (Figure 2a). The Rietveld refinement using the RIETAN-FP grogram[57] gives the lattice parameters of a_{hex}= b_{hex}=2.96785(2) Å and c_{hex}=16.27990(9) Å. The other refined

COMMUNICATION

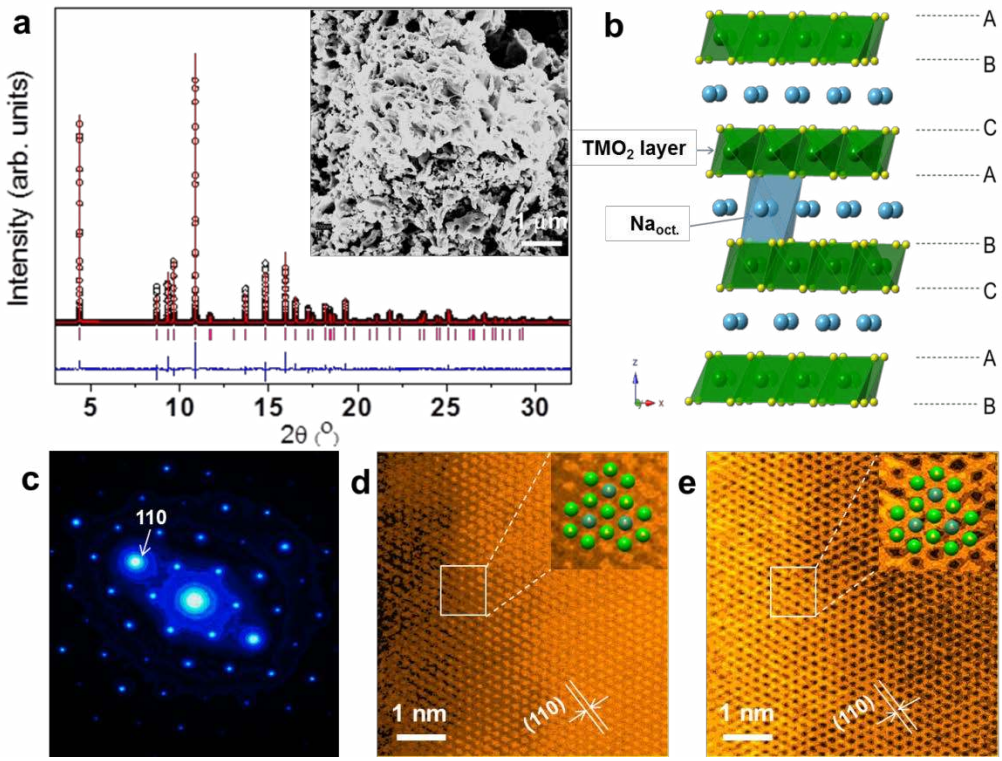

Figure 2. The structural characterization of O3-type $Na_{0.8}Ni_{0.4}Ti_{0.6}O_2$ materials **(a)** HR-SXRD pattern and Rietveld refinement of layered $Na_{0.8}Ni_{0.4}Ti_{0.6}O_2$ material. A red line represents the observed intensities; The calculated pattern is shown with black circles; The difference between the observed and calculated intensities is presented by a blue curve; Pink short vertical bars indicate the position of standard Bragg reflections. The inset shows SEM image of $Na_{0.8}Ni_{0.4}Ti_{0.6}O_2$ samples. **(b)** Schematic illustration of the crystal structure for O3-type $Na_{0.8}Ni_{0.4}Ti_{0.6}O_2$. **(c)** The SAED patterns **(d)** HADDF and **(e)** ABF-STEM images of $Na_{0.8}Ni_{0.4}Ti_{0.6}O_2$ samples projected along [001] direction. The insets of **(d)** and **(e)** in top-right corners shows sodium (blue balls) and transition metal (green balls) occupancies.

structural parameters are summarized in Table S1 and S2. The calculated patterns (circles in Figure 2a) were in good agreement with experimental data (red lines in Figure 2a), indicative of a pure O3-type structure, isostructural with α-$NaFeO_2$. The scanning electron microscopy (SEM) image in the inset of Figure 2a, reveals that layered $Na_{0.8}Ni_{0.4}Ti_{0.6}O_2$ samples consist of interconnected primary particles with a size of about 100-500 nm. A schematic illustration of the structure model of O3-type $Na_{0.8}Ni_{0.4}Ti_{0.6}O_2$ is presented in Figure 2b. In this model, nickel and titanium ions are accommodated in the octahedral sites of TMO_2 layer (3a sites, TM = Ni and Ti), while sodium ions are located in the octahedral sites of NaO_2 layer (3b sites). The detailed crystal structure is further investigated by Selected Area Electron Diffraction (SAED) techniques. The bright spots in Figure S1a and Figure 2c are indexed to the corresponding reflections originating from O3-type layered structure. Atomic-resolution investigation on the local structure of layered $Na_{0.8}Ni_{0.4}Ti_{0.6}O_2$ samples was also conducted by High-angle Annular Dark Field (HAADF) and Annular Bright Field (ABF) Scanning Transmission Electron Microscopy (STEM) techniques (Figure. 2d and 2e). The bright-dot contrast in the HAADF-STEM images (Figure 2d) and the dark-dot contrast in ABF-STEM images (Figure 2e) reveal the sodium and transition metal (Ni and Ti) atom positions, and sodium is fully overlapped by transition metal projected along [001] direction, which is consistent with O3-type layered structure. High Resolution Transmission Electron Microscope (HR-TEM) characterization further suggests the interlayer spacing about 0.555 nm of (003) fringes in O3-type $Na_{0.8}Ni_{0.4}Ti_{0.6}O_2$ (Figure S1b).

Electrochemical properties of O3-type $Na_{0.8}Ni_{0.4}Ti_{0.6}O_2$ as bipolar material are characterized by cyclic voltammetry (CV) and galvanostatic charge-discharge or discharge-charge test in the half cells vs. Na^+/Na, shown in Figure 3. The CV curve in the green part of Figure 3a reflects an oxidation peak at 3.7 V and a weak reduction hump at 3.5 V, attributable to the redox couples of Ni^{4+}/Ni^{2+} and possible phase change. Upon charging to 4 V with the initial charge capacity of 107 mAh g^{-1} in Figure S2a (exceeding the theoretical capacity based on Ni^{3+}/Ni^{2+} redox couples), the desodiated $Na_{0.8-x}Ni_{0.4}Ti_{0.6}O_2$ samples was conducted with X-ray Photoelectron Spectroscopy (XPS) experiment in Figure S2b. A clear shoulder peak corresponding to Ni^{4+} (857.4 eV) was detected, which validates

COMMUNICATION

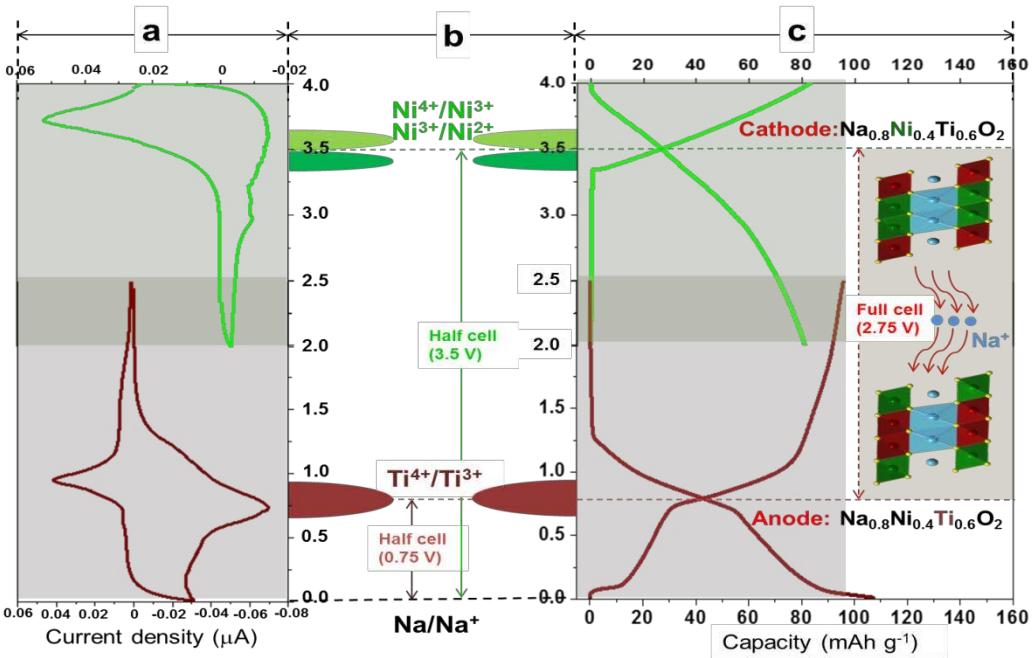

Figure 3. The electrochemical performance of the O3-type $Na_{0.8}Ni_{0.4}Ti_{0.6}O_2$ in the half cell *vs.* Na^+/Na **(a)** The CV curves of O3-type $Na_{0.8}Ni_{0.4}Ti_{0.6}O_2$ in the voltage range of 2-4 V for Ni^{4+}/Ni^{2+} (green) and 0.01-2.5 V for Ti^{4+}/Ti^{3+} (brown) *vs.* Na^+/Na. **(b)** Schematic of potential of the Ni^{4+}/Ni^{3+}, Ni^{3+}/Ni^{2+} and Ti^{4+}/Ti^{3+} redox couples *vs.* Na/Na^+ in layered $Na_{0.8}Ni_{0.4}Ti_{0.6}O_2$ materials. The insets display the average potentials of the $Na_{0.8}Ni_{0.4}Ti_{0.6}O_2$/Na half cells as cathode and anode, respectively. **(c)** The typical charge-discharge or discharge-charge profiles of the $Na_{0.8}Ni_{0.4}Ti_{0.6}O_2$/Na half cells in the voltage range of 2-4 V (green) and 0.01-2.5 V (brown) *vs.* Na^+/Na. The inset (yellow parts) shows the predicted average voltage of 2.8 V in the bipolar $Na_{0.8}Ni_{0.4}Ti_{0.6}O_2$-based symmetric cells.

the proposed Ni^{4+}/Ni^{2+} redox mechanism. It is known that the tetravalent nickel is unstable in the cells' disassembly process or the XPS test procedure, and is easier to change and transfer, so a small number of tetravalent nickel ions are observed in our ex-situ XPS result. Accordingly, the green part of Figure 3c shows the voltage profile for the typical (second) charge-discharge cycle from 2 to 4 V vs. Na^+/Na at a 0.2 C rate, demonstrating that the electrode delivers a capacity of 83 mAh g^{-1}. The charge-discharge curve displays a reversible, distinct plateau of 3.5 V, well agreeable with the CV curves. The cycle stability is further investigated with $Na_{0.8}Ni_{0.4}Ti_{0.6}O_2$ half cells in Figure S3. It delivers a large reversible capacity of 63 mAh g^{-1} at a rate of 1C, corresponding to 76% of discharge capacity at a 0.2C rate with small polarization. Also, $Na_{0.8}Ni_{0.4}Ti_{0.6}O_2$ shows good cycle performance，and the capacity still maintains 47 mAh g^{-1} after 250 cycles, the corresponding capacity retention is 75%, and the Coulombic efficiency is close to 100% except for the first cycle. Compared with layered $NaNiO_2$ with single transition metal, the multi-step character of charge and discharge profiles is clearly suppressed and even disappeared in the titanium-substituted $Na_{0.8}Ni_{0.4}Ti_{0.6}O_2$, replaced by the smooth charge-discharge profiles.[27, 41, 42] The detailed structural change with sodium extraction and insertion will be investigated in the subsequent section.

The CV curve in the brown part of Figure 3a shows the distinct redox peak about 0.7 V, which is attributed to the redox of Ti^{4+}/Ti^{3+}. Accordingly, the typical (second) discharge-charge profile is displayed in the brown part of Figure 3c, and the observed reversible capacity is 107 mAh g^{-1}, along with an obvious step around 0.7 V, which is also validated by the CV curve. The cycle stability and Coulombic efficiency are also evaluated in Figure S4. The revesible capacity at a 1C rate can still maintains 62 mAh g^{-1}, and corresponds to about 58% discharge capacity of 0.2C rate. Also the capacity retention after 250 cycles is 86% and Coulombic efficiency except for initial cycles can reach nearly 100% in all the charge-discharge processes (Figure S4). In contrary to layered O3-type $NaTiO_2$, nickel-substituted $Na_{0.8}Ni_{0.4}Ti_{0.6}O_2$ shows excellent structural stability with cycling, which is expected that nickel substitution greatly improve the titanium ions stability in the transition metal layers.[39, 44] The structure stability will further be proved by the subsequent ex-situ XRD structural evolution analysis in the discharge-charge process.

Figure 3b shows the schematic of electric potential for the Ni^{4+}/Ni^{2+} and Ti^{4+}/Ti^{3+} redox couples in O3-type $Na_{0.8}Ni_{0.4}Ti_{0.6}O_2$, corresponding to the average voltage of $Na_{0.8}Ni_{0.4}Ti_{0.6}O_2$/Na half cells. On the basis of their voltage difference, the average potential of this symmetric cell using the bipolar active material

COMMUNICATION

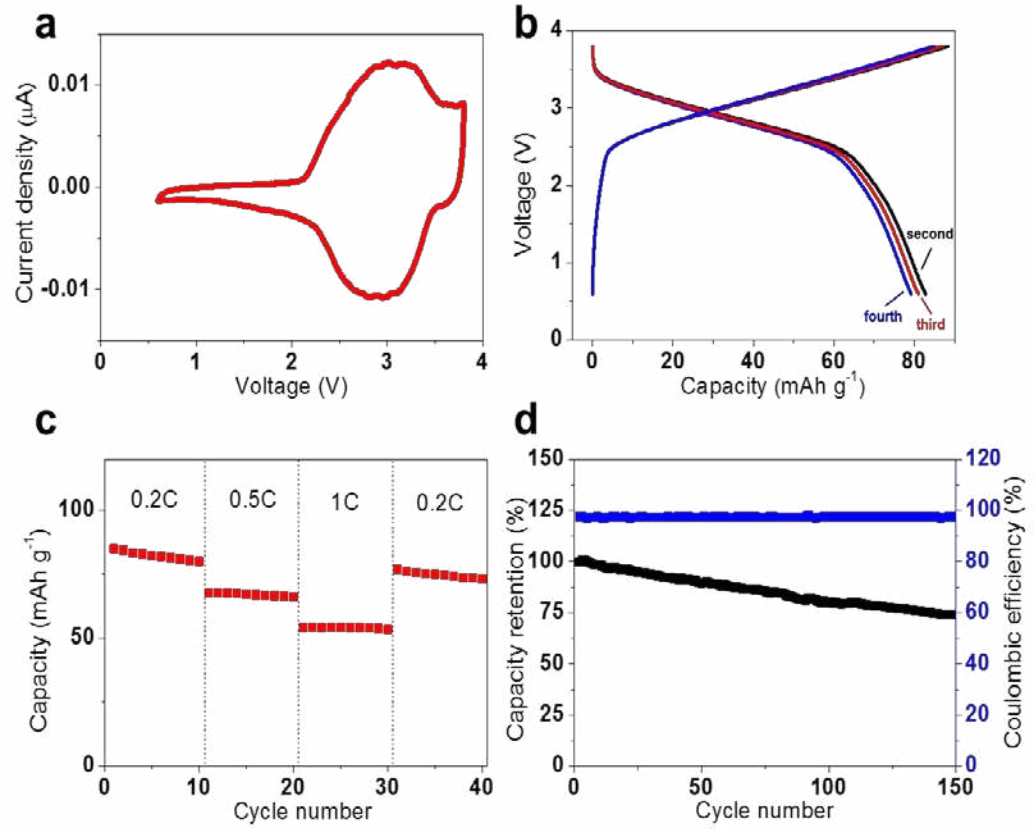

Figure 4. The electrochemical performance of bipolar $Na_{0.8}Ni_{0.4}Ti_{0.6}O_2$-based symmetric cells. **(a)** The CV curve in the voltage range of 0.6-3.8 V. **(b)** The typical charge-discharge profiles in the voltage range of 0.6-3.8 V. **(c)** The rate capability at different rates of 0.2C, 0.5C and 1C. **(d)** The cycling performance with Coulombic efficiency at a 1C rate.

$Na_{0.8}Ni_{0.4}Ti_{0.6}O_2$ is predicted, shown in the inset of Figure 3c. Different from O3-type $Na_{0.8}Ni_{0.4}Ti_{0.6}O_2$, P2-type $Na_{2/3}Ni_{1/3}Ti_{2/3}O_2$ only with the cathode and anode performances in sodium half cells have been investigated.[21] And some properties are also compared in Table S3.

In order to depress the polarization and irreversibility effect of $Na_{0.8}Ni_{0.4}Ti_{0.6}O_2$ in the first charge process (cathode side) and discharge process (anode side), the pre-desodiated and pre-sodiated $Na_{0.8}Ni_{0.4}Ti_{0.6}O_2$ are used as positive and negative electrode materials in the sodium full cells. Full batteries containing desodiated and sodiated $Na_{0.8}Ni_{0.4}Ti_{0.6}O_2$ were characterized using CV and galvanostatic cyling. Figure 4a illustrates the CV curve of the full cell with the optimized voltage range of 0.6-3.8 V. An oxidation peak with average voltage of 3.0 V and a reduction peak with average voltage of 2.8 V were observed, which is consistent with the predicted value in Figure 3c. A reversible discharge capacity of 85 mAh g^{-1} was obtained in the first cycle (Figure S5) and subsequent cycles (Figure 4b) at a charge-discharge rate of 0.2 C. As shown in Figure 4b, the charge-discharge profile displays symmetrical characteristic, and it is clearly seen that no obvious polarization is observed in this well-configured symmetric full cells. The rate capability is also evaluated with different charge-discharge rates of 0.2C, 0.5C and 1C in Figure 4c. The reversible capacity can be 67 mAh g^{-1} at a 0.5C rate, and even with the rate of 1C, the discharge capacity remains 53 mAh g^{-1}, approximately 62% of the reversible capacity at a 0.2C rate. With a rate of 1C, the symmetric battery offers 75% of capacity retention for extensive cycling of 150 times sodium extraction and insertion, and the corresponding Coulombic efficiency is exceeding 97% except for the initial cycle (Figure 4d).

To understand the reaction mechanism of O3-type $Na_{0.8}Ni_{0.4}Ti_{0.6}O_2$ during sodium insertion and extraction processes, we performed the ex-situ XRD and STEM experiments in the $Na_{0.8}Ni_{0.4}Ti_{0.6}O_2$/Na half cell. Figure S6a shows the initial charge-discharge profile, in which the green points are denoted for ex-situ XRD and STEM test. It is evident that the initial phase is O3-type rhombohedral (Figure S6b, point 1), and the patterns of O3 layered structure broaden, weaken with desodiation and a new phase appears (Figure S6b, point 2). This phase is assigned to P3-type monoclinic,[58-60] having an interlayer distance larger than that of O3-

type layer structure, continues to strengthen and become the dominant after the full desodiation (Figure S6b, point 3). It is also validated by the intensity ratio of $(104)_{hex}$ and $(105)_{hex}$ diffraction (the intensity of the $(104)_{hex}$ diffraction line is stronger for O3 phase, while that of the $(105)_{hex}$ line is stronger for P3 layered structure) in Figure S6b.[61] In order to distinguish P3 phase from O3 phase, the expanded view of ex-situ XRD patterns is shown in Figure S6c. In the P3 phase, Na is in trigonal prismatic coordination, which is simply caused by the $TMO_2^{\delta-}$ layers with less negative charge so that the trigonal prismatic environment is favored over the octahedral one.[45, 60] On discharge, the P3-type monoclinic phase remains at the partial sodiation and mostly transforms back into the original O3-type layer structure (Figure S6c, point 5). And the O3 structure dominates with a weak peaks belonging to P3 structure (Figure S6c, point 5), and the schematic of the O3-P3 phase transition was shown in Figure S7. SAED and HAADF and ABF-STEM tests projected along $[1\ \bar{1}\ 0]$ direction were also conducted in the desodiated materials after charge to 4V (Figure S6a, point 3). Figure S6d is the corresponding SAED pattern, and bright spots are indexed to the corresponding reflection of P3 layered structure. Owing to the phase transition from O3 to P3 and structural distortion, it is difficult to detect the atom occupancies in P3 layered structure and the increased interlayer spacing of 0.566 nm corresponding to (003) fringes is observed in Figure S6e and S6f.

Figure S8a displays the first discharge-charge profile in the $Na_{0.8}Ni_{0.4}Ti_{0.6}O_2$/Na half cell, in which the brown points are denoted for ex-situ XRD and STEM test. All peaks are unchanged, shift weakly with sodium insertion and extraction (Figure S8b), demonstrating the high structural stability during cycling. No other distinct new phase is generated during the first cycle, suggesting that this structure is flexible enough to accommodate the structural changes accompanying the extraction and insertion of the large sodium ions in a low potential area. Otherwise, the sample at discharge of 0.01 V displays the typical bright spots corresponding to the corresponding reflection originating from O3 layered structure in the SAED patterns (Figure S8c). HAADF and ABF-STEM images of Figure S8d and S8e suggest that the layered spacing of the (003) fringes decreases to 0.546 nm and the typical sodium and transition metal occupancies completely overlap with typical O3 structure, which further verified the structural stability in sodium extraction and insertion process.

Differential scanning calorimetry (DSC) with this bi-polar material at different conditions is conducted to investigate the thermal stability, shown in Figure S9. The pristine $Na_{0.8}Ni_{0.4}Ti_{0.6}O_2$ shows no obvious exothermic peaks, indicating good thermal stability. And the exothermic temperatures of deeply desodiated materials (charging to 4 V as cathode) and sodiated materials (discharging to 0.01 V as anode), which are 364 °C and 345 °C respectively, appear higher than that of another layered sodium oxide.[45] The high thermal stability at deeply desodiated and sodiated conditions probably contributes to the presence of stable TiNi layers in the crystal framework of this bi-polar material.

In summary, a novel, symmetric sodium-ion battery delivers a maximum 96 Wh kg^{-1} based on the massed of cathode and anode materials at a 0.2C rate, as well as performing an exceeding 75% capacity retention over a hundred and fifty cycles at a 1C charge-discharge rate. These properties, together with the good rate capability, low active material cost and the recycling convenience make this unique battery system more attractive for grid-related applications. Further work on the symmetric batteries optimization by substituting nickel with other transition metal is currently under investigation.

Experimental

Material preparation.

O3-type $Na_{0.8}Ni_{0.4}Ti_{0.6}O_2$ raw materials are synthesized by solid-state reaction. All solid chemical compounds were purchased from Wako Pure Chemicals Industries Ltd.. The precursors of Na_2CO_3, NiO and TiO_2 (anatase form) are well ground in an agate mortar at a rotate rate of 200 r/min for 20 h. Owing to the sodium volatility in high temperature, an access 5 wt.% of Na_2CO_3 is added. The mixture is dried for 12 h at 100 °C. The obtained powders were pressed into pellets, and then the pellets were heated at 900 °C for 15 h in the Ar flow. The heated pellets were quenched to room temperature and stored in an argon-filled glove box until use.

Characterizations.

The HR-SXRD patterns were collected in a transmission mode at the beam line 11-BM-B of the Advanced Photon Source, Argonne National Laboratory, USA. A monochromatic X-ray beam with an energy of 30 keV (wavelength of 0.413742 Å) was used. The ex-situ XRD patterns were performed using Cu Kα radiation on a Bruker D8 Advance Diffractometer. The detailed structural information of as-prepared materials was also observed using scanning electron microscopy (SEM, TOPCON DS-720 instrument) and Cs-corrected transmission electron microscope (TEM, JEOL, JEM-2010 and JEM-2100F). The charged cathodes scratched from the electrodes of sodium half cells were subjected to XPS on a VG Theta Probe. Thermal stability was examined by differential scanning calorimetry (DSC) on EXSTAR 7000 X-DSC in a temperature range of 50-400 °C at a heating rate of 10 °C min^{-1}. Before DSC measurements, the cells were firstly charged to 4.0 V or discharged at 0.01 V at a current of 20 mA g^{-1}. After that, the cells were disassembled in an Ar filled glove box, the charged or discharged samples were collected and sealed in Al-pan for DSC measurements.

Electrochemistry.

The electrochemical tests of $Na_{0.8}Ni_{0.4}Ti_{0.6}O_2$/Na half cells were carried out using the CR2032 coin-type cells, consisting of a cathode and sodium metal anode separated by a glass fiber. The cathode electrodes were prepared with a weight ratio of 70% of active material, 25% of teflonized acetylene black, and 5% of polytetrafluoroethylene. Pellets for half cells were pressed in the form of aluminium screens approximately 3 mg in mass and 7 mm in diameter (the loading mass is around 1.95 mg cm^{-2}), then dried under vacuum at about 110 °C for 5 h before cells assembly. The cells were assembled in a glove box filled with dried argon gas. The electrolyte was 1 mol dm^{-3} $NaClO_4$ dissolved in propylene carbonate (Tomiyama Pure Chemical Industries) with 2 vol% fluorinated ethylene carbonate as an electrolyte additive. The $Na_{0.8}Ni_{0.4}Ti_{0.6}O_2$/Na half cells were cycled in the voltage range of 2-4 V for cathode performance and 0.01-2.5 V for anode performance. Prior to full cells fabrication, the pre-sodiation of $Na_{0.8}Ni_{0.4}Ti_{0.6}O_2$ anode and pre-desodiation of $Na_{0.8}Ni_{0.4}Ti_{0.6}O_2$ cathode were performed to carry out the first cycle activation. The cell balance was achieved by setting the electrode mass ratio of cathode/anode to 1.4 (the anode loading mass is around 1.95 mg cm^{-2}). The full cell is then anode limited and is reassembled and cycled in the voltage of 0.6-3.8 V. 1C corresponds to 100 mA g^{-1} for all the cell tests.

Notes and references

[a] *Energy Technology Research Institute, National Institute of Advanced industrial Science and Technology (AIST), Japan; Fax: +81-29-861-3489; Tel: +81-29-861-5795; E-mail: hs.zhou@aist.go.jp, haijun-yu@aist.go.jp*
[b] *Graduate School of System and Information Engineering, University of Tsukuba, Tennoudai 1-1-1, Tsukuba, 305-8573, Japan*
[c] *WPI Advanced Institute for Materials Research, Tohoku University, Sendai 980-8577, Japan.*
[d] *Argonne National Laboratory, 9700 South Cass Avenue, Argonne, Illinois, 60439, USA.*
[e] *National Laboratory of Solid State Microstructures & Department of Energy Science and Engineering, Nanjing University, Nanjing 210093, China*

Electronic Supplementary Information (ESI) available: See DOI: 10.1039/c000000x/

1. B. Dunn, H. Kamath and J.-M. Tarascon, *Science*, 2011, **334**, 928-935.
2. Z. Yang, J. Zhang, M. C. Kintner-Meyer, X. Lu, D. Choi, J. P. Lemmon and J. Liu, *Chemical Reviews*, 2011, **111**, 3577-3613.
3. J. Liu, J. G. Zhang, Z. Yang, J. P. Lemmon, C. Imhoff, G. L. Graff, L. Li, J. Hu, C. Wang and J. Xiao, *Advanced Functional Materials*, 2013, **23**, 929-946.
4. J.-M. Tarascon and M. Armand, *Nature*, 2001, **414**, 359-367.
5. J. B. Goodenough and Y. Kim, *Chemistry of Materials*, 2009, **22**, 587-603.
6. H.-G. Jung, M. W. Jang, J. Hassoun, Y.-K. Sun and B. Scrosati, *Nature communications*, 2011, **2**, 516.
7. S. W. Lee, N. Yabuuchi, B. M. Gallant, S. Chen, B.-S. Kim, P. T. Hammond and Y. Shao-Horn, *Nature Nanotechnology*, 2010, **5**, 531-537.
8. C. K. Chan, H. Peng, G. Liu, K. McIlwrath, X. F. Zhang, R. A. Huggins and Y. Cui, *Nature nanotechnology*, 2007, **3**, 31-35.
9. B. Kang and G. Ceder, *Nature*, 2009, **458**, 190-193.
10. H. Pan, Y.-S. Hu and L. Chen, *Energy & Environmental Science*, 2013, **6**, 2338-2360.
11. M. Pasta, C. D. Wessells, R. A. Huggins and Y. Cui, *Nature communications*, 2012, **3**, 1149.
12. N. Yabuuchi, M. Kajiyama, J. Iwatate, H. Nishikawa, S. Hitomi, R. Okuyama, R. Usui, Y. Yamada and S. Komaba, *Nature materials*, 2012, **11**, 512-517.
13. P. Barpanda, G. Oyama, C. D. Ling and A. Yamada, *Chemistry of Materials*, 2014, **26**, 1297-1299.
14. S. Wang, L. Wang, Z. Zhu, Z. Hu, Q. Zhao and J. Chen, *Angewandte Chemie*, 2014, **126**, 6002-6006.
15. J. Qian, X. Wu, Y. Cao, X. Ai and H. Yang, *Angewandte Chemie*, 2013, **125**, 4731-4734.
16. D. Su and G. Wang, *ACS nano*, 2013, **7**, 11218-11226.
17. W.-J. Li, S.-L. Chou, J.-Z. Wang, H.-K. Liu and S.-X. Dou, *Nano letters*, 2013, **13**, 5480-5484.
18. Y. You, X.-L. Wu, Y.-X. Yin and Y.-G. Guo, *Energy & Environmental Science*, 2014, **7**, 1643-1647.
19. Y. Yan, Y. X. Yin, Y. G. Guo and L. J. Wan, *Advanced Energy Materials*, 2014.
20. D. Kim, S. H. Kang, M. Slater, S. Rood, J. T. Vaughey, N. Karan, M. Balasubramanian and C. S. Johnson, *Advanced Energy Materials*, 2011, **1**, 333-336.
21. R. Shanmugam and W. Lai, *ECS Electrochemistry Letters*, 2014, **3**, A23-A25.
22. Z. Jian, W. Han, X. Lu, H. Yang, Y. S. Hu, J. Zhou, Z. Zhou, J. Li, W. Chen and D. Chen, *Advanced Energy Materials*, 2013, **3**, 156-160.
23. Y.-U. Park, D.-H. Seo, H.-S. Kwon, B. Kim, J. Kim, H. Kim, I. Kim, H.-I. Yoo and K. Kang, *Journal of the American Chemical Society*, 2013, **135**, 13870-13878.
24. S. Y. Lim, H. Kim, J. Chung, J. H. Lee, B. G. Kim, J.-J. Choi, K. Y. Chung, W. Cho, S.-J. Kim and W. A. Goddard, *Proceedings of the National Academy of Sciences*, 2014, **111**, 599-604.
25. K. H. Ha, S. H. Woo, D. Mok, N. S. Choi, Y. Park, S. M. Oh, Y. Kim, J. Kim, J. Lee and L. F. Nazar, *Advanced Energy Materials*, 2013, **3**, 770-776.
26. Y. Yue, A. J. Binder, B. Guo, Z. Zhang, Z. A. Qiao, C. Tian and S. Dai, *Angewandte Chemie*, 2014, **126**, 3198-3201.
27. H.-W. Lee, R. Y. Wang, M. Pasta, S. W. Lee, N. Liu and Y. Cui, *Nature communications*, 2014, **5**.
28. B. Jache and P. Adelhelm, *Angewandte Chemie International Edition*, 2014, **53**, 10169-10173.
29. S. Komaba, W. Murata, T. Ishikawa, N. Yabuuchi, T. Ozeki, T. Nakayama, A. Ogata, K. Gotoh and K. Fujiwara, *Advanced Functional Materials*, 2011, **21**, 3859-3867.
30. M. S. Islam and C. A. Fisher, *Chemical Society Reviews*, 2014, **43**, 185-204.
31. R. Tripathi, S. M. Wood, M. S. Islam and L. F. Nazar, *Energy & Environmental Science*, 2013, **6**, 2257-2264.
32. Y. Mo, S. P. Ong and G. Ceder, *Chemistry of Materials*, 2014, **26**, 5208-5214.
33. M. Guignard, C. Didier, J. Darriet, P. Bordet, E. Elkaïm and C. Delmas, *Nature materials*, 2013, **12**, 74-80.
34. C.-Y. Chen, K. Matsumoto, T. Nohira, R. Hagiwara, A. Fukunaga, S. Sakai, K. Nitta and S. Inazawa, *Journal of Power Sources*, 2013, **237**, 52-57.
35. X. Ma, H. Chen and G. Ceder, *Journal of The Electrochemical Society*, 2011, **158**, A1307-A1312.
36. J. Zhao, L. Zhao, N. Dimov, S. Okada and T. Nishida, *Journal of The Electrochemical Society*, 2013, **160**, A3077-A3081.
37. R. Berthelot, D. Carlier and C. Delmas, *Nature materials*, 2011, **10**, 74-80.
38. P. Vassilaras, X. Ma, X. Li and G. Ceder, *Journal of The Electrochemical Society*, 2013, **160**, A207-A211.
39. A. Maazaz, C. Delmas and P. Hagenmuller, *Journal of inclusion phenomena*, 1983, **1**, 45-51.
40. J. Billaud, G. Singh, A. R. Armstrong, E. Gonzalo, V. Roddatis, M. Armand, T. Rojo and P. G. Bruce, *Energy & Environmental Science*, 2014, **7**, 1387-1391.
41. D. Stevens and J. Dahn, *Journal of the Electrochemical Society*, 2000, **147**, 1271-1273.
42. Y. Cao, L. Xiao, M. L. Sushko, W. Wang, B. Schwenzer, J. Xiao, Z. Nie, L. V. Saraf, Z. Yang and J. Liu, *Nano letters*, 2012, **12**, 3783-3787.
43. D. Kim, E. Lee, M. Slater, W. Lu, S. Rood and C. S. Johnson, *Electrochemistry Communications*, 2012, **18**, 66-69.
44. Y. Wang, X. Yu, S. Xu, J. Bai, R. Xiao, Y.-S. Hu, H. Li, X.-Q. Yang, L. Chen and X. Huang, *Nature communications*, 2013, **4**.
45. S.-M. Oh, S.-T. Myung, C. S. Yoon, J. Lu, J. Hassoun, B. Scrosati, K. Amine and Y.-K. Sun, *Nano letters*, 2014, **14**, 1620-1626.
46. L. S. Plashnitsa, E. Kobayashi, Y. Noguchi, S. Okada and J.-i. Yamaki, *Journal of the Electrochemical Society*, 2010, **157**, A536-A543.
47. P. Senguttuvan, G. Rousse, M. Arroyo y de Dompablo, H. Vezin, J.-M. Tarascon and M. Palacín, *Journal of the American Chemical Society*, 2013, **135**, 3897-3903.
48. S. Li, Y. Dong, L. Xu, X. Xu, L. He and L. Mai, *Advanced Materials*, 2014.
49. E. Kobayashi, L. S. Plashnitsa, T. Doi, S. Okada and J.-i. Yamaki, *Electrochemistry Communications*, 2010, **12**, 894-896.
50. Y. Noguchi, E. Kobayashi, L. S. Plashnitsa, S. Okada and J.-i. Yamaki, *Electrochimica Acta*, 2013, **101**, 59-65.
51. J. Braconnier, C. Delmas and P. Hagenmuller, *Materials Research Bulletin*, 1982, **17**, 993-1000.
52. M. H. Han, E. Gonzalo, M. Casas-Cabanas and T. Rojo, *Journal of Power Sources*, 2014, **258**, 266-271.
53. H. Yu, S. Guo, Y. Zhu, M. Ishida and H. Zhou, *Chemical Communications*, 2014, **50**, 457-459.
54. H. Yu, Y. Ren, D. Xiao, S. Guo, Y. Zhu, Y. Qian, L. Gu and H. Zhou, *Angewandte Chemie*, 2014.
55. Y.-J. Shin and M.-Y. Yi, *Solid State Ionics*, 2000, **132**, 131-141.
56. Y.-J. Shin, M.-H. Park, J.-H. Kwak, H. Namgoong and O. H. Han, *Solid State Ionics*, 2002, **150**, 363-372.
57. Y. Shimakawa, Y. Kubo, Y. Nakagawa, S. Goto, T. Kamiyama, H. Asano and F. Izumi, *Physical Review B*, 2000, **61**, 6559.

58. S. Komaba, T. Nakayama, A. Ogata, T. Shimizu, C. Takei, S. Takada, A. Hokura and I. Nakai, *ECS Transactions*, 2009, **16**, 43-55.
59. S. Komaba, N. Yabuuchi, T. Nakayama, A. Ogata, T. Ishikawa and I. Nakai, *Inorganic chemistry*, 2012, **51**, 6211-6220.
60. M. Sathiya, K. Hemalatha, K. Ramesha, J.-M. Tarascon and A. Prakash, *Chemistry of Materials*, 2012, **24**, 1846-1853.
61. I. Saadoune, A. Maazaz, M. Ménétrier and C. Delmas, *Journal of Solid State Chemistry*, 1996, **122**, 111-117.

COMMUNICATION

TOC

Novel symmetric sodium-ion batteries based on bipolar materials O3-type $Na_{0.8}Ni_{0.4}Ti_{0.6}O_2$ are well configured, showing better good capability and capacity retention.

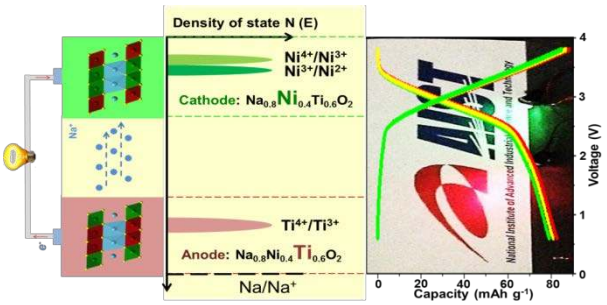

Broader context: With the increasing concerns on fossil fuels depletion and environmental issues, green and sustainable energy such as wind and solar power has been tremendously developed in the modern electrical grid. When lithium-ion batteries (LIBs) technology poised to move into large scale applications, the limited lithium availability and rapid-increase cost would not be suited for the substantial demand. Rechargeable sodium-ion batteries (SIBs) with similar chemical storage mechanism represent the most appealing alternative to their lithium-ion counterparts, and are expected to be low-cost and chemically sustainable due to almost infinite supply of sodium. In this work, we report an interesting symmetric sodium-ion battery based on a new bipolar active material O3-type $Na_{0.8}Ni_{0.4}Ti_{0.6}O_2$. By using two electrochemically active transition metals with redox couples of Ni^{4+}/Ni^{2+} and Ti^{4+}/Ti^{3+} respectively, this $Na_{0.8}Ni_{0.4}Ti_{0.6}O_2$-based symmetric cell exhibits a high voltage of 2.8 V, a reversible discharge capacity of 85 mAh g^{-1}, 75% capacity retention after 150 cycles and good rate capability.